PROCEEDINGS, Thirty-Ninth Workshop on Geothermal Reservoir Engineering
Stanford University, Stanford, California, February 24-26, 2014
SGP-TR-202

Multi-Fluid Geothermal Energy Systems in Stratigraphic Reservoirs: Using Brine, N_2, and CO_2 for Dispatchable Renewable Power Generation and Bulk Energy Storage

Thomas A. Buscheck[1], Jeffrey M. Bielicki[2], Jimmy B. Randolph[3], Mingjie Chen[1], Yue Hao[1], Thomas A. Edmunds[1], Benjamin Adams[3] and Yunwei Sun[1]

[1]Atmospheric, Earth, and Energy Division, Lawrence Livermore National Laboratory (LLNL)
P.O. Box 808, L-223, Livermore CA 94550, USA
buscheck1@llnl.gov

[2]Department of Civil and Geodetic Engineering, The Ohio State University (OSU), Columbus, OH USA
[3]Department of Earth Sciences, University of Minnesota, Minneapolis, MN USA

Keywords: Sedimentary basins, bulk energy storage, geologic CO_2 sequestration, horizontal wells, parasitic load, dispatchable power

ABSTRACT

Stratigraphic reservoirs are attractive candidates for geothermal power production due to their high permeability and large areal extent, compared to typical hydrothermal geothermal reservoirs. Because they are often associated with a conductive thermal regime that require greater depths to reach economic temperatures, the commercial viability of stratigraphic reservoir systems will depend on leveraging greater fluid production rates per well and on limiting the parasitic costs associated with fluid recirculation. We present an approach to address these challenges. To increase fluid-recirculation efficiency and fluid production rates, we inject supplemental working fluids (CO_2 and/or N_2) with advantageous properties to augment reservoir pressure. Because N_2 can be readily separated from air, pressure augmentation can occur during periods of low grid power demand, which will reduce parasitic costs and enable bulk energy storage. A well pattern consisting of four concentric rings of horizontal producers and injectors is used to store pressure and supplemental fluids, segregate the supplemental fluid and brine production zones, and generate large artesian flow rates to better leverage the productivity of horizontal wells. We present simulations of this approach for an idealized reservoir model, consisting of a permeable sedimentary formation, vertically confined by two impermeable seal units. Because the parasitic costs associated with compressing and injecting supplemental fluids and brine increase with reservoir overpressure, net power production is found to be more efficient at moderate supplemental-fluid injection rates.

1. INTRODUCTION

Stratigraphic reservoirs in sedimentary basins are attractive candidates for geothermal power production because they have the advantages of higher reservoir permeability, with much of that permeability being in the rock matrix rather than fractures, and much larger areal extent, compared to hydrothermal systems in crystalline rock formations where conventional geothermal power systems are usually deployed. However, these reservoirs are typically associated with a conductive thermal regime, requiring greater depths to reach economic temperatures than hydrothermal upflows. Because of their high permeability, these basins are being targeted for geologic CO_2 sequestration (GCS). The NATCARB Regional Carbon Sequestration Partnership (RCSP) database (Carr et al., 2007) has identified extensive regions suitable for GCS. A significant subset of this area has high enough temperature to be of economic value for CO_2-based geothermal energy production (Elliot et al., 2013). Stratigraphic reservoirs also have lower, predictable drilling risk. These make an attractive target for geothermal development, but several challenges need to be addressed. Primary challenges are to maximize heat extraction and power generation on a per well basis, while minimizing the parasitic costs of fluid recirculation.

CO_2 enhanced geothermal energy systems (EGS), a geothermal concept using CO_2 instead of water as the working fluid, was first proposed by Brown (2000). Pruess (2006) followed up on his idea by analyzing reservoir behavior and found CO_2 to be superior to water in mining heat from hot fractured rock, including reduced parasitic power consumption to drive the fluid recirculation system. This concept has been extended to GCS in sedimentary formations (Randolph and Saar, 2011a; 2011b; 2011c; Saar et al., 2010), which they call a CO_2-Plume Geothermal (CPG) system, to distinguish it from CO_2-based EGS in crystalline rock. Because it is targeted for large, porous, permeable sedimentary basins, CPG can result in more CO_2 sequestration and more heat extraction than CO_2-based EGS in crystalline rock.

While most research on CO_2-based geothermal systems has emphasized using CO_2 as a working fluid (Pruess, 2006; Randolph and Saar, 2011a; 2011b, 2011c; Saar et al., 2010), it is possible to expand on this idea by using CO_2 as a pressure-support fluid to generate artesian pressures to drive brine production (Buscheck et al., 2013a). To address the high cost of CO_2 captured from fossil-fueled power plants, and to provide operational flexibility, we have further broadened this approach with the addition of N_2 as a supplemental working fluid (Buscheck et al., 2013b; Buscheck, 2014). N_2 is advantageous because it can be separated from air at low cost, compared to CO_2, it is non-corrosive and will not react with the formation, and has no raw material supply risk. If injected prior to (or with) CO_2, N_2 can mitigate possible operational issues associated with CO_2, such as flashing in the wellbore.

2. MULT-FLUID GEOTHERMAL ENERGY SYSTEMS

To increase fluid-recirculation efficiency and per well fluid production rates, supplemental fluids (CO_2 and/or N_2) are injected to augment reservoir pressure and to add working fluids with advantageous properties, such as their low viscosities and high coefficients of thermal expansion. Pressure augmentation is improved by the thermosiphon effect that results from injecting cold/dense CO_2 and N_2 (Adams et al., 2014). These fluids are heated to reservoir temperature, greatly expand, and thus increase the artesian flow of brine and supplemental fluid at the production wells. Because N_2 can be readily separated from air, pressure augmentation can occur during periods of low power demand or when there is a surplus of renewable energy on the grid, which will reduce parasitic costs associated with fluid recirculation and enable bulk energy storage. Our approach uses a well pattern consisting of a minimum of four concentric rings of horizontal producers and

injectors (Figure 1) that creates a hydraulic divide designed to store pressure and supplemental fluids much like a hydroelectric dam, segregate the supplemental fluid and brine production zones, and generate large artesian flow rates to better leverage the productivity of horizontal wells. Because fluid production is driven by stored pressure, it is possible to schedule production to coincide when power demand is high or when there is a deficit of renewable energy on the grid. The hydraulic divide segregates the inner swept zone, where brine and supplemental fluid recirculate, from the outer swept zone, where only brine recirculates.

The combined benefits of geothermal power generation and bulk energy storage may render this approach commercially viable if it is sited in a sedimentary basin with two key attributes: (1) a caprock with large enough contiguous area and low enough permeability to confine vertical migration of the buoyant supplemental-fluid (CO_2 and/or N_2) plume and (2) a pay-zone compartment with enough area and permeability to allow lateral hydraulic communication between widely spaced rings of injection and production wells without requiring large overpressures. Other beneficial attributes include limited faulting and faults with limited vertical offsets within the pay-zone compartment. The commercial viability of a site should increase with pay-zone transmissivity. Viability should also improve with compartment volume, area, and thickness.

3. MODELING APPROACH

Reservoir analyses were conducted with the NUFT code, which simulates multi-phase heat and mass flow and reactive transport in porous media (Nitao, 1998; Hao et al., 2012). The pore and water compressibility are 4.5×10^{-10} and 3.5×10^{-10} Pa^{-1}, respectively. Water density is determined by the ASME steam tables (ASME, 2006). The two-phase flow of supercritical CO_2 and water was simulated with the density and compressibility of supercritical CO_2 determined by the correlation of Span and Wagner (1996) and viscosity determined by the correlation of Fenghour et al. (1997). The two-phase flow of supercritical N_2 and water was simulated with the density and compressibility for N_2 determined by correlation of Span et al. (2000) and the viscosity determined by the correlation of Lemmon and Jacobsen (2004).

A generic system is modeled, consisting of a 250-m-thick reservoir with a permeability of 1×10^{-13} m^2, bounded by impermeable (caprock and bedrock) seal units with a permeability of 1×10^{-18} m^2. Hydrologic properties (Table 1) are similar to previous GCS and GCS-geothermal studies (Zhou et al., 2008; Buscheck et al., 2012a; 2012b; 2013a; 2013b; Elliot et al., 2013). Because conditions are assumed to be laterally homogeneous, we can use a radially-symmetric (RZ) model. A geothermal gradient of 37.5°C/km and reservoir bottom depths of 3, 4, and 5 km are considered. The initial temperature at the bottom of the reservoir is 127.0, 164.5, and 202.0°C for these cases, respectively, assuming an average surface temperature of 14.5°C. The RZ model is representative of rings of arc-shaped horizontal wells. Using an RZ model allows for fine mesh refinement, particularly around the injectors and producers to better model pressure gradients close to the wells.

Table 1: Hydrologic and thermal properties used in this study.

Property	Reservoir	Seal units (caprock and bedrock)
Permeability (m^2)	1.0×10^{-13}	1.0×10^{-18}
Thermal conductivity (W/m°C)	2.0	2.0
Porosity	0.12	0.12
van Genuchten (1980) *m*	0.46	0.46
van Genuchten α (1/Pa)	5.1×10^{-5}	5.1×10^{-5}
Residual supercritical fluid saturation	0.05	0.05
Residual brine saturation	0.30	0.30

With respect to supplemental fluid injection, NUFT is used to model two cases: (1) pure supercritical CO_2 injection and (2) pure supercritical N_2 injection. We use the reservoir model results to determine brine-based, Organic Rankine Cycle binary-power generation, using the GETEM code (DOE, 2012). Geothermal energy is extracted from produced CO_2 and N_2 at the surface using a direct-cycle power system, in which the produced CO_2 and/or N_2 is itself sent through a turbine rather than a binary-power system. For CO_2 and N_2 working fluids, direct-power systems offer much greater energy conversion efficiency than binary systems because the supercritical fluids generate a substantial pressure difference between the hot production wellhead and the cold injection wellhead, while simultaneously losing considerable temperature during their rise in production wells. The latter effect – Joule-Thomson cooling – causes low binary-system efficiency compared to brine-based systems operating at similar reservoir temperatures. We assume that produced brine has been separated from the produced CO_2 and/or N_2 prior to sending those fluids through the turbine for power extraction. Because the energy penalty for fluid separation is minor, we have neglected it from our power-generation analyses.

Recent studies of multi-fluid geothermal power systems have considered a CO_2 injection rate (480 kg/sec) that would be associated with CO_2 captured from large fossil-energy power plants (Buscheck et al., 2013a; 2013b). To address such a large CO_2 injection rate, the four-ring well pattern had a radius of 9 km for the outer brine producer ring, with a well-field footprint area of 255 km^2. For this study, we considered smaller well-field footprint areas of 64 and 129 km^2 (one quarter to one half of that considered earlier, as shown in Table 2). For this study we also considered two radial spacings (0.5 and 1.0 km) between the two rings of injectors. Table 2 summarizes the geometries of the four cases considered in this study. Important quantities are the inner swept area, which is where the supplemental fluid (CO_2 or N_2) recirculates and where fluid displacement generates "excess" brine to be reinjected in the third well ring, and the outer swept area, which is where brine is recirculated. Ideally, the ratio of the outer to inner swept areas could be chosen to yield similar rates of thermal decline in the respective swept zones. A large inner swept area will delay the breakthrough of supplemental fluid at the inner production ring, thereby displacing more brine that is available for reinjection in the third well ring, which increases the rate of thermal decline at the outer brine produces. A large inner swept area also tends to delay thermal decline at the inner producers. A relatively small inner swept area tends to have the opposite effects of those described above.

For this study we considered a wide range of supplemental-fluid (CO_2 and N_2) injection rates (30 to 480 kg/sec). We assumed that all of the produced supplemental fluid is reinjected, up to a limit of twice the initial supplemental-fluid injection rate. Thus, the case with an initial injection rate of 480 kg/sec could have an injection rate up to 960 kg/sec. Restricting the maximum supplemental-fluid injection rate eventually limits the amount of N_2 or CO_2 that has to be delivered to maintain that injection rate. All of the

produced brine is reinjected into the brine injectors in ring 3. For sufficiently small injection rates, CO_2 or N_2 never reaches the inner producers and the supplemental-fluid injection rate remains fixed at the initial value.

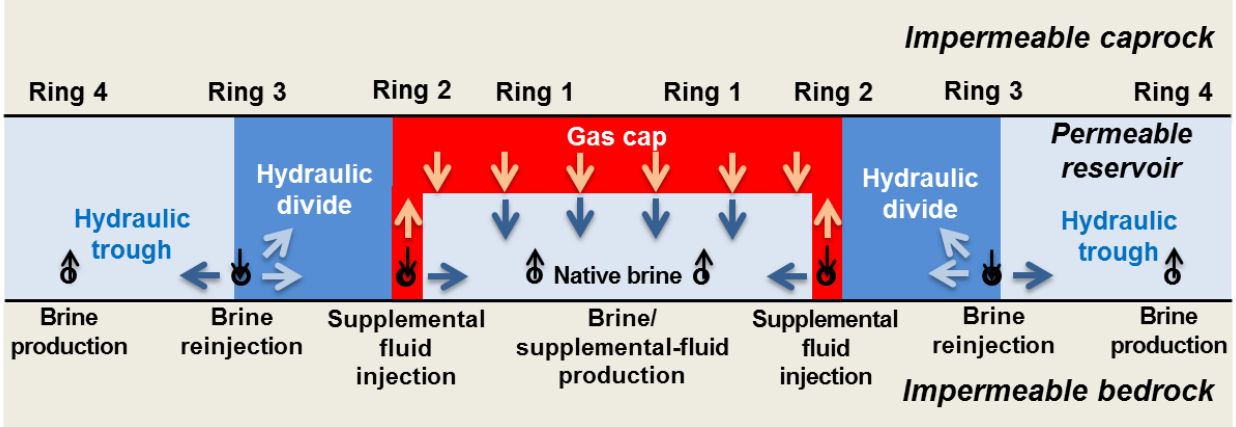

Figure 1: Schematic of a multi-ring well-field configuration used in multi-fluid geothermal energy systems (Buscheck, 2014). For this study, all wells were located at the bottom of the permeable reservoir formation. Due to buoyancy, supplemental fluid (CO_2 or N_2) will quickly migrate to top of the permeable reservoir and form a "gas" cap.

Table 2: Four-ring well-field cases considered in this study.

Well-field footprint area (km^2)	Well-ring radius (km)				Radial spacing between injector rings (km)	Inner swept area (km^2)	Outer swept area (km^2)	Notes
	Ring 1 brine/CO_2/N_2 producers	Ring 2 CO_2/N_2 injectors	Ring 3 brine injectors	Ring 4 brine producers				
64	0.5	2.0	2.5	4.5	0.5	11.8	44.0	Large ΔP, medium thermal decline
64	0.5	2.0	3.0	4.5	1.0	11.8	35.4	Reduced ΔP, rapid thermal decline
129	0.5	2.9	3.4	6.4	0.5	25.6	92.4	Small ΔP, slow thermal decline
129	0.5	2.9	3.9	6.4	1.0	25.6	80.9	Small ΔP, slow thermal decline
255	2.0	4.0	6.0	9.0	2.0	37.7	141.5	Buscheck et al (2013a; 2013b)

4. RESULTS

The results are presented in three parts. We begin in Section 4.1, analyzing power generation and energy storage for specific cases, including initial N_2 injection rates of 240 and 120 kg/sec. In Section 4.2, we analyze power generation for initial CO_2 injection rates of 240 and120 kg/sec, and compare that with the corresponding N_2 injection cases. In Section 4.3, we analyze the dependence of power generation and parasitic load to supplemental-fluid injection rate for a wide range of CO_2 and N_2 injection rates. We also consider the influence of reservoir depth and temperature.

4.1 Power Generation and Energy Storage with N_2 Injection

Figure 2 plots the distributions of gas saturation of N_2, reservoir overpressure, and temperature at 30 yr for an initial N_2 injection rate of 240 kg/sec, a reservoir bottom depth of 5 km, a well-field footprint area of 129 km^2, and 0.5-km radial spacing between the N_2 and brine injection rings. The influence of buoyancy on N_2 migration is evident (Figure 2a). Note that N_2 breakthrough has already occurred at the inner ring of producers prior to year 30. The hydraulic divide is evident in the distribution of overpressure (Figure 2b). The temperature distribution (Figure 2c) shows that thermal breakthrough has occurred at the outer ring of brine producers; however, very little thermal decline is evident at the inner ring of producers. Table 3 breaks down the contributions of parasitic load on net power. For this case, the parasitic power load to compress N_2 is 1.94 %, while the parasitic load to separate N_2 from air is 4.85%. The largest parasitic load (20.33%) is that required to compress brine for reinjection into the overpressured reservoir (Figure 2b), assuming a pump efficiency of 80%.

Figures 3a and c plot the history of brine production and overpressure at the N_2 injector for a corresponding case with an initial N_2 injection rate of 120 kg/sec, along with two corresponding energy-storage cases:

- 20-day energy-storage cycle: 10 days of 240-kg/sec N_2 injection, followed by 10 days of no injection.
- 1-yr energy-storage cycle: 3 months of 480-kg/sec N_2 injection, followed by 9 months of no injection.

For the 20-day energy-storage cycle, the influence of cyclic N_2 injection is hardly apparent in brine production, N_2 injector overpressure, and net power histories. Gross power, parasitic load, and net power are virtually the same for the no-storage and 20-day storage cycle case over the 30-yr production period (Table 3). For the 1-yr energy-storage cycle, the influence of cyclic N_2 injection is clearly evident in the brine production, N_2 injector overpressure, and net power histories. However, gross power, parasitic load, and net power are very similar between the no-storage and energy-storage cases over the 30-yr production period (Table 3).

We also analyzed energy storage for well-field footprint half of this area (64 km^2). Because there is roughly half as much cushion gas, cyclic fluctuations of brine production, N_2 injection overpressure, and net power histories are greater than in the 129-km^2 case (Figure 3b and d). However, gross power, parasitic load, and net power are nearly the same between the no-storage and energy-storage cases (Table 3).

As shown in Table 3, we considered a wide range of energy-storage cases using N_2 injection. For all cases considered, time-shifting the parasitic load of N_2 separation and pumping never resulted in any loss of geothermal power generation capacity. Time-shifting the parasitic load of N_2 separation and pumping results in the ranges of energy storage rate (71.73 to 375.52 MWe) and of stored energy per cycle (18.08 to 333.91 GWe-hr) listed in Table 3.

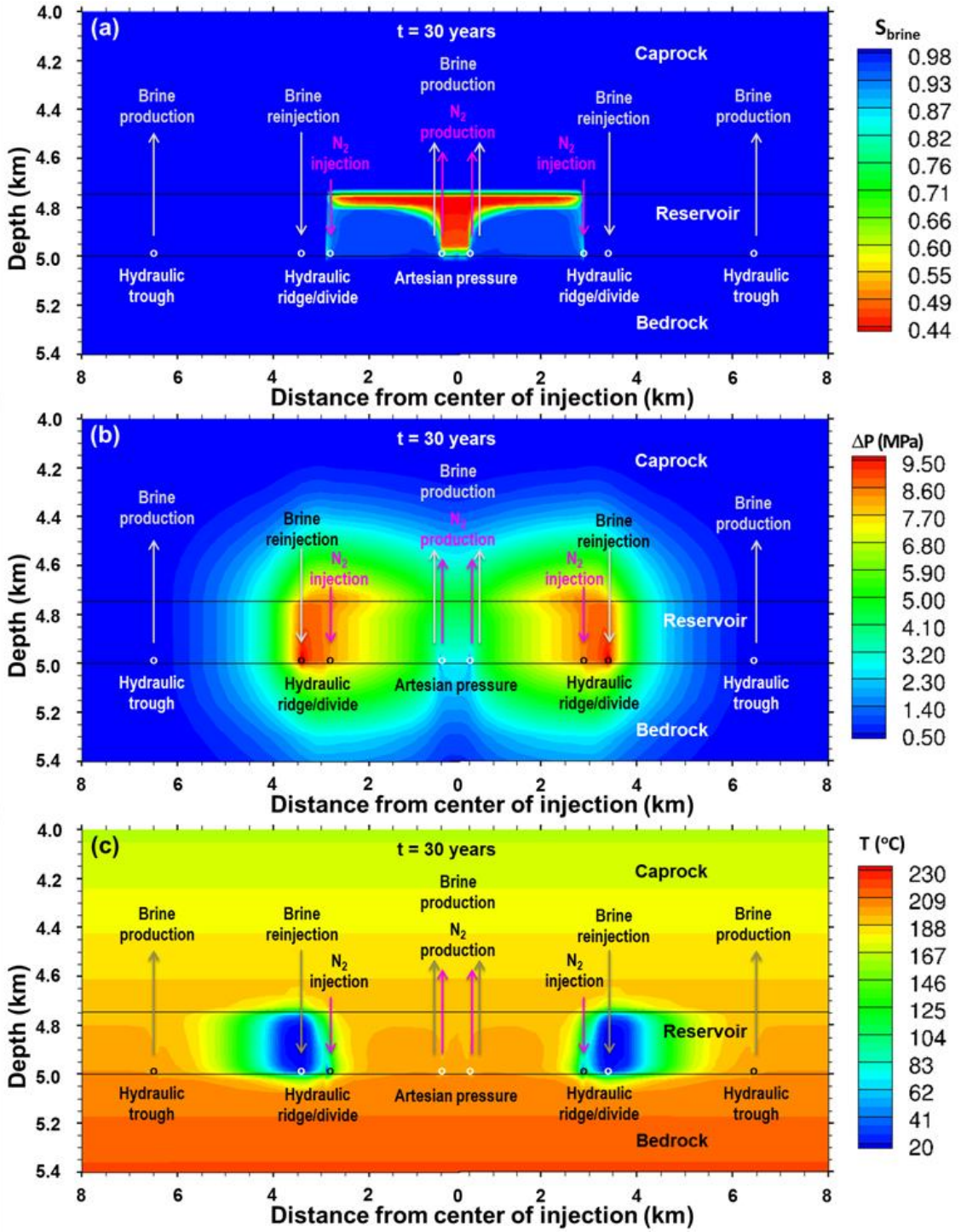

Figure 2: Gas saturation S_{gas} (a), overpressure ΔP (b), and temperature (^oC) are plotted at 30 yr for an initial N_2 injection rate of 240 kg/sec, a reservoir bottom depth of 5 km, a well-field footprint area of 129 km^2, and 0.5-km radial injector-ring spacing.

4.2 Power Generation with CO_2 Injection

Figure 4 plots the distributions of gas saturation of CO_2 and reservoir overpressure at 30 yr for an initial CO_2 injection rate of 240 kg/sec, a reservoir bottom depth of 5 km, a well-field footprint area of 129 km^2, and 0.5-km radial spacing between the CO_2 and brine injection rings. The distributions are qualitatively similar to those in the corresponding N_2 injection case. The extent of the CO_2 plume is smaller because its density is nearly twice that of N_2 (compare Figure 4a with Figure 3a). Because there is less volumetric displacement of brine, overpressure is less than in the N_2 case (compare Figure 4b with Figure 3b) and the thermally swept zone is also smaller (compare Figure 4c with Figure 3c), which reduces the rate of thermal decline for the outer ring of brine producers.

Returning to the case with an initial supplemental-fluid injection rate of 120 kg/sec, we find that CO_2 injection generates less gross power than the corresponding N_2 injection case (Table 3) because the higher density of CO_2 displaces less brine and generates less overpressure than N_2. The parasitic load to compress CO_2 is much less than that of N_2 because of the higher density of CO_2. Due to the lower overpressure in the CO_2 case, it takes less compression to inject the produced brine, which results in a smaller parasitic load for brine pumping. Overall, the lower parasitic load compensates for the lower gross power output, resulting in nearly the same net power output as in the N_2 injection case (Table 3).

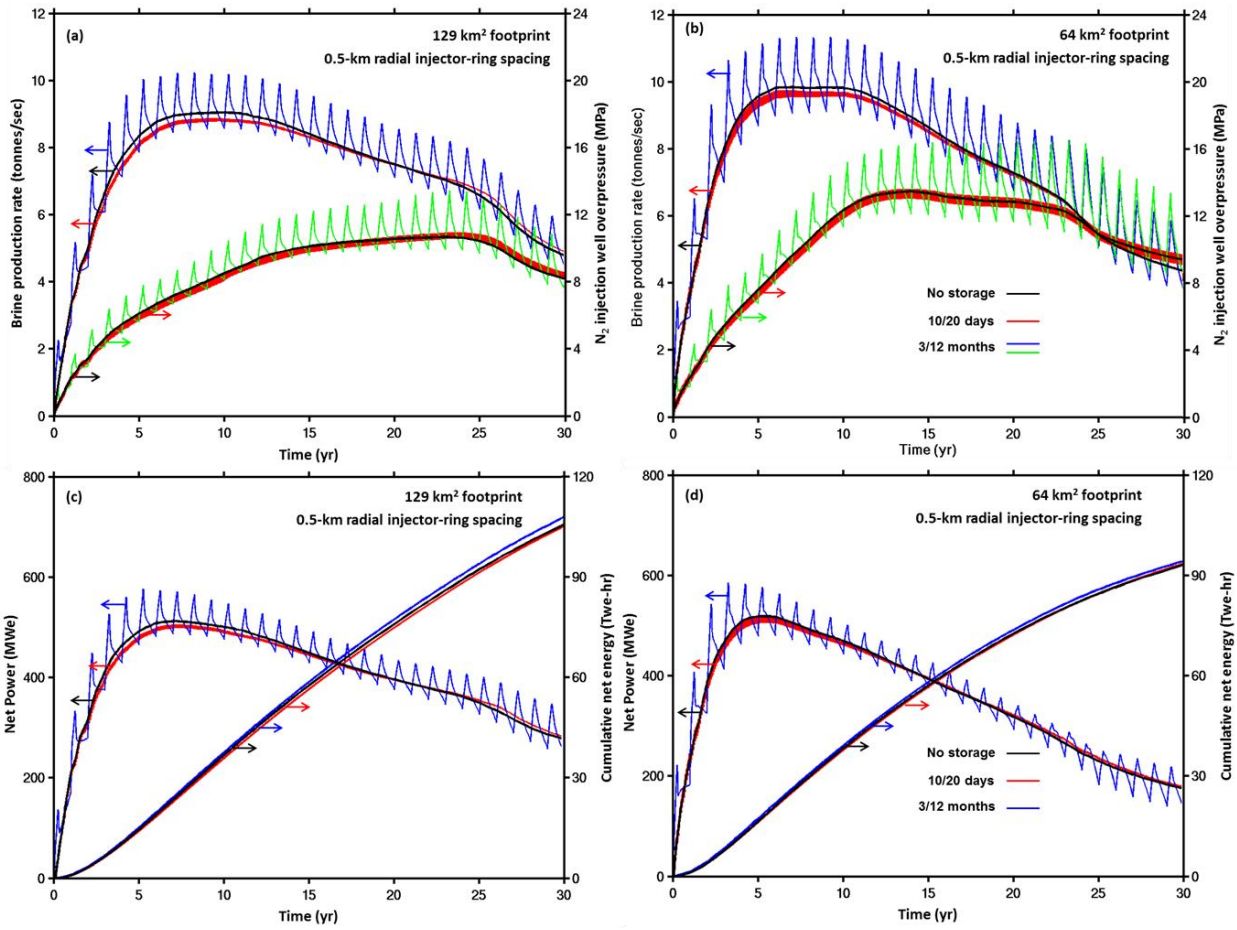

Figure 3: Histories of brine production rate, N_2 injection well overpressure, net power generation rate, and cumulative energy are plotted for a well-field footprint of 129 km^2 (a,c) and 64.3 km^2 (b,d). For all cases, the average initial N_2 injection rate is 120 kg/sec, reservoir bottom depth is 5 km, and radial injector-ring spacing is 0.5 km. Cases are plotted for no energy storage (constant 120-kg/sec N_2 injection) and two energy-storage cases: (1) 10 days of 240-kg/sec N_2 injection, followed by 10 days of no injection and (2) 3 months of 480-kg/sec N_2 injection, followed by 9 months of no injection.

Table 3: Summary of power over a 30-yr period for the energy-storage cases considered in this study, using time-shifted N_2 separation and injection. A corresponding no-storage case with CO_2 injection is included for comparison. All cases have an initial average initial supplemental-fluid injection rate of 120 kg/sec.

Production footprint area (km^2)	Energy storage cycle (injection/ total)	Energy storage rate (MWe)	Energy stored per cycle (GWe-hr)	Power (MWe)		Parasitic load (%)		
				Gross	Net	N_2 (or CO_2) pumping	N_2 separation	Brine pumping
129	No storage CO_2 injection	NA	NA	442.00	374.12	0.21	NA	15.15
	No storage	NA	NA	551.89	402.26	1.94	4.85	20.33
	10/20 days	75.33	18.08	548.54	400.23	1.96	4.91	20.17
	100/200 days	75.56	180.69	546.10	398.68	1.96	4.96	20.08
	50/200 days	150.11	179.42	553.77	403.13	1.92	4.86	20.43
	20/200 days	375.52	179.55	553.84	403.09	1.92	4.86	20.44
	3/12 months	152.37	333.91	569.02	411.27	1.90	4.80	21.17
64	No storage CO_2 injection	NA	NA	452.89	358.79	0.22	NA	20.56
	No storage	NA	NA	543.77	354.36	2.05	4.56	28.22
	10/20 days	71.73	17.22	541.82	355.73	2.08	4.54	27.73
	100/200 days	72.35	172.95	533.62	353.54	2.23	4.55	26.97
	50/200 days	148.57	177.58	571.08	359.08	1.87	4.63	30.29
	20/200 days	361.04	172.62	547.52	356.40	2.03	4.57	28.31
	3/12 months	148.40	325.18	564.21	358.47	1.96	4.62	29.89

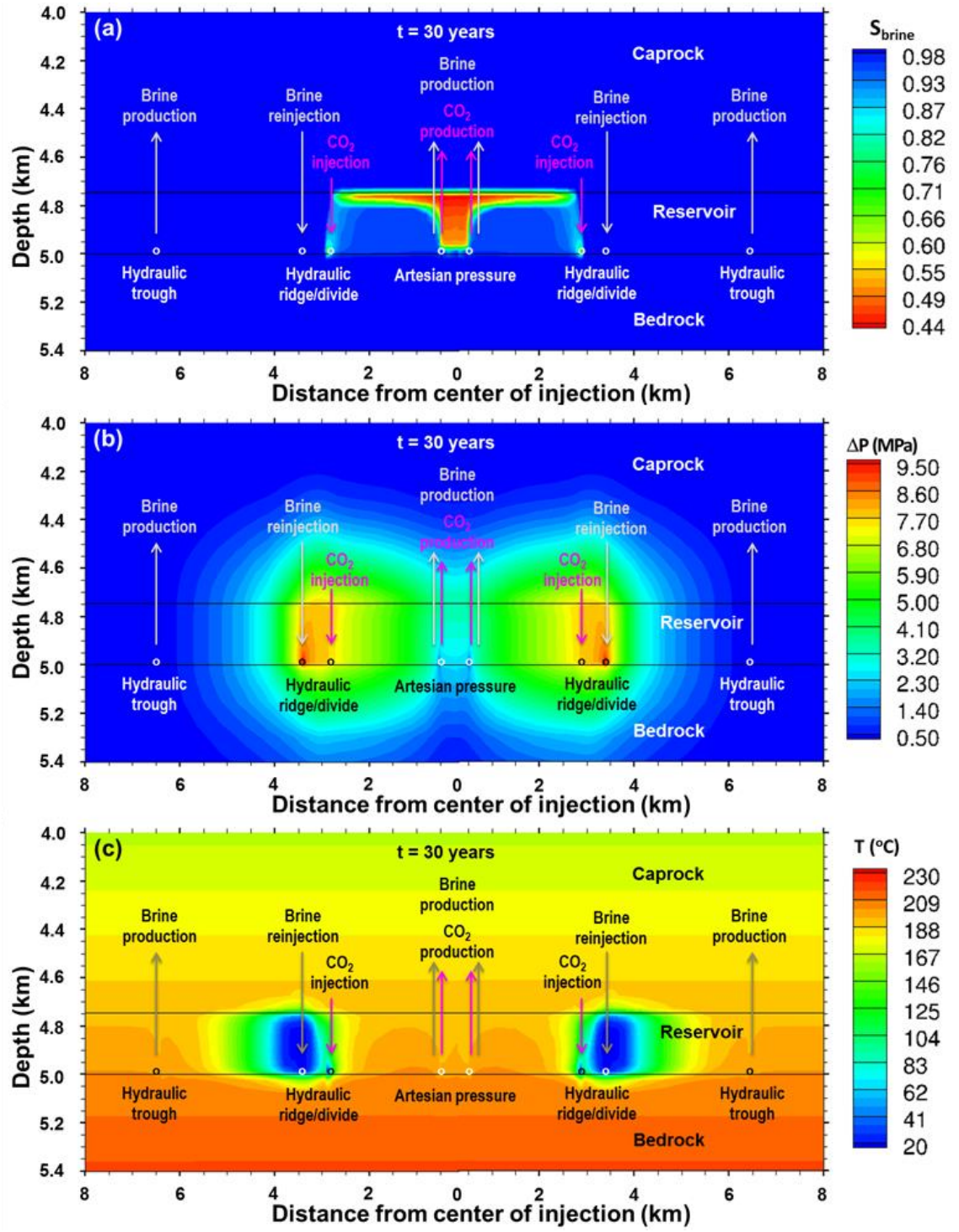

Figure 4: Gas saturation S_{gas} (a), overpressure ΔP (b), and temperature (°C) are plotted at 30 yr for an initial CO_2 injection rate of 240 kg/sec, a reservoir bottom depth of 5 km, a well-field footprint area of 129 km^2, and 0.5-km radial injector-ring spacing.

4.3 Dependence of Power Generation and Parasitic Load on Supplemental-Fluid Injection Rate and Reservoir Depth

Figure 5 is a summary of power performance over the 30-year production period for initial supplemental-fluid injection rates ranging from 30 to 480 kg/sec for all cases with 0.5-m radial spacing between the injector rings. Figure 6 summarizes the corresponding production temperature for the outer production ring and the peak brine injector overpressure. Several striking trends are apparent.

- For a well-field footprint area of 64 km^2, net power grows weakly with increasing CO_2 injection rate for rates greater than 120 kg/sec (Figure 5a). This trend is due to temperature declining with increasing CO_2 injection rate (Figure 6a).

- For a well-field footprint area of 64 km^2, net power is nearly flat or declines with increasing N_2 injection rate for rates greater than 120/sec (Figure 5b). This trend is due to temperature declining strongly with increasing N_2 injection rate (Figure 6b). This trend is also due to the fact that N_2 generates less gross power than is required for N_2 compression and reinjection for temperatures less than 164.5°C. Thus, it is counterproductive to produce N_2 for reservoir depths of 3 and 4 km. For those situations, N_2 should only be used to augment pressure for brine production, not to be used as a working fluid for heat extraction.

- For a well-field footprint area of 129 km^2, net power increases with both CO_2 and N_2 injection rate (Figures 5a and b). Net power for CO_2 increases more strongly because CO_2 is a more efficient working fluid than N_2 for gross power output and because of its lower parasitic load, compared to N_2 (Table 3). Thus, increasing the contribution of CO_2 production (Figure 5c) is a cost-effective means of boosting net power output. The trends for CO_2 and N_2 are also due to the negligible temperature decline over the 30-yr production period (Figures 6a and b) for the 129-km^2 footprint.

- The contribution of supplemental-fluid production to net power increases with supplemental-fluid injection rate (Figures 5e and f). As discussed above, this is useful for CO_2 production; however, it is only marginally useful for N_2 production for the high reservoir temperature associated with the reservoir bottom depth of 5 km. For reservoir bottom depths of 3 and 4 km, increased N_2 production is counterproductive (Figure 5b).

- Peak overpressure decreases strongly with decreasing supplemental-fluid injection rate for rates less than 120 kg/sec (Figures 6c and d). Above 120 kg/sec, peak overpressure increases less strongly with supplemental-fluid injection rate. This trend is due to the influence of supplemental-fluid breakthrough at the inner producers has on relaxing overpressure (Figures 5e and f). For this well configuration, a *spill-point* effect occurs at a supplemental-fluid injection rate of ~120 kg/sec. For rates below this threshold, most of the injected supplemental fluid is stored; pressurizing the reservoir inside injection well rings 2 and 3 (Figures 2b and 3b). Above this threshold, supplemental-fluid production relieves much of the incremental overpressure.

- The unit value of CO_2 and N_2, defined to be equal to total 30-yr power sales at $0.10/KWe-hr divided by the 30-yr net storage of either CO_2 or N_2, strongly increases with decreasing supplemental-fluid injection rate for rates less than 120 kg/sec. For an initial CO_2 injection rate of 30 kg/sec, the unit value of CO_2 ranges from $54 to $196/tonne, depending on reservoir depth and temperature. Such a range of unit CO_2 value could justify the cost of CO_2 capture, provided geothermal operations were scaled to the magnitude of CO_2 capture rates associated with typical fossil-energy power plants (~120 kg/sec).

- Parasitic load depends strongly on overpressure (compare Figures 5c and d with Figures 6c and d), due to the power required to pressurize brine for reinjection. Because overpressure strongly depends on supplemental-fluid injection rate below the spill-point threshold value, parasitic load decreases strongly with decreasing supplemental-fluid injection rate below this threshold.

- Parasitic load increases strongly with decreasing reservoir depth and temperature (Figures 5 c and d). This trend is due to thermal decline resulting in uneconomic temperatures being reached during the latter portion of the 30-yr production period. Parasitic load is particularly high for high N_2 injection rates and low reservoir temperature, due to N_2 being an inefficient carrier of heat at lower temperature. For low reservoir temperature, it is particularly important for N_2 injection rates to be low enough to limit thermal decline and to avoid N_2 production. At an initial supplemental-fluid injection rates below 60 kg/sec, N_2 injection is just as effective as CO_2 injection in generating net power for the reservoir depth of 3 km (compare Figures 5a and b).

In light of the preceding observations, we modified the well-field configuration by increasing the radial spacing between the injector rings from 0.5 to 1.0 km (Figures 7 and 8), which broadened the width of the hydraulic ridge, thereby reducing the magnitude of overpressure by nearly a third (compare Figures 8c and d with Figures 6c and d). Broadening the width of the hydraulic ridge resulted in several striking trends.

- The reduction in overpressure reduced the parasitic load for both CO_2 and N_2 (compare Figures 7c and d with Figures 5c and d).

- For a well-field footprint area of 64 km^2, thermal decline is steeper than in the 0.5-km radial injector-ring spacing (compare Figures 8a and b with Figures 5a and b). Broadening the radial injector-ring spacing reduces the outer swept area between the brine injectors and outer ring brine producers by 20 % (Table 2), resulting in earlier thermal breakthrough.

- For a well-field footprint area of 64 km^2, net power is nearly the same as in the 0.5-km radial injection-ring spacing cases for reservoir bottom depths of 4 and 5 km due to the offsetting influence of decreased parasitic load and more rapid thermal decline. For a reservoir bottom depth of 3 km, net power is improved because the reduction in parasitic load was more pronounced (compare Figures 7c and d with Figures 5c and d).

- Doubling well-field footprint area from 64 to 129 km^2 significantly boosts net power due to the much slower thermal decline rate (Figures 8a and b); thus, the beneficial influence of reduced overpressure-driven parasitic load is not diminished by thermal decline, as it was for the 64-km^2 well-field footprint area. Doubling of the well-field footprint area significantly boosts net power for all three reservoir bottom depths (Figures 7a and b).

An important and perhaps non-intuitive finding of this study is that it does not require much supplemental fluid (CO_2 or N_2) to substantially enhance the rate of brine production and power generation. The obvious benefit of CO_2 and N_2 injection is that it generates excess brine for reinjection through displacement; however, there is an additional, more subtle, and more profound benefit of this injection process, which is altering the pressure distribution within the reservoir. We find that a relatively small amount of CO_2 or N_2 can create a "topographic high" in pressure, which allows overpressured brine to be injected in the third ring of wells "uphill" from the "downhill" outer brine producers (Figures 3b and 4b). This process is the subsurface equivalent of pumped-storage hydroelectricity. Subsurface "pumped storage" will drive brine production and generate highly dispatchable power, without requiring submersible pumps to lift brine. Large centralized pumps located on the surface are likely to be more efficient that submersible pumps. Surface-based pumps would not be exposed to the harsh conditions in the brine producers and not require the frequent maintenance that would disrupt production. Pumped storage could be particularly valuable in hydrostatic reservoirs where temperatures are too hot (> 200°C) for submersible pumps to survive and operate. Where long-reach horizontal wells are used, pumped storage could result in flow rates much greater than the capacity of submersible pumps (80 to 120 kg/sec), which would increase leveraging of well costs.

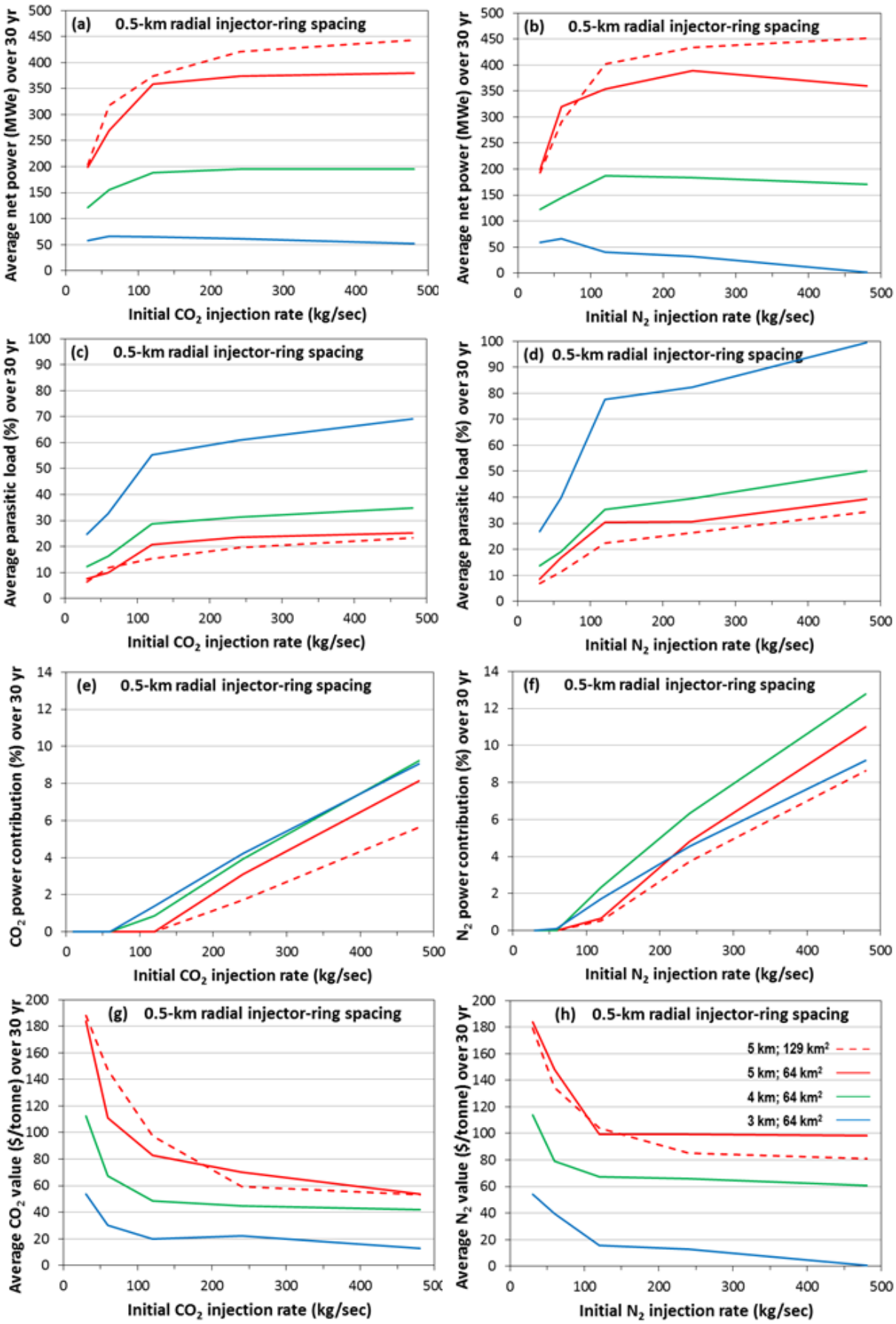

Figure 5: Power summary for CO_2 injection (a,c,e,g) and N_2 injection (b,d,f,h) for cases with 0.5-km radial injector ring spacing. Cases are included for reservoir bottom depths of 3, 4, and 5 km, and well-field footprint areas of 64 and 129 km^2. The power summary is plotted for initial CO_2 and N_2 injection rates ranging from 30 to 480 kg/sec. The average unit CO_2 and N_2 values are based on total power sales at $0.10/KWe-hr over a period of 30 yr.

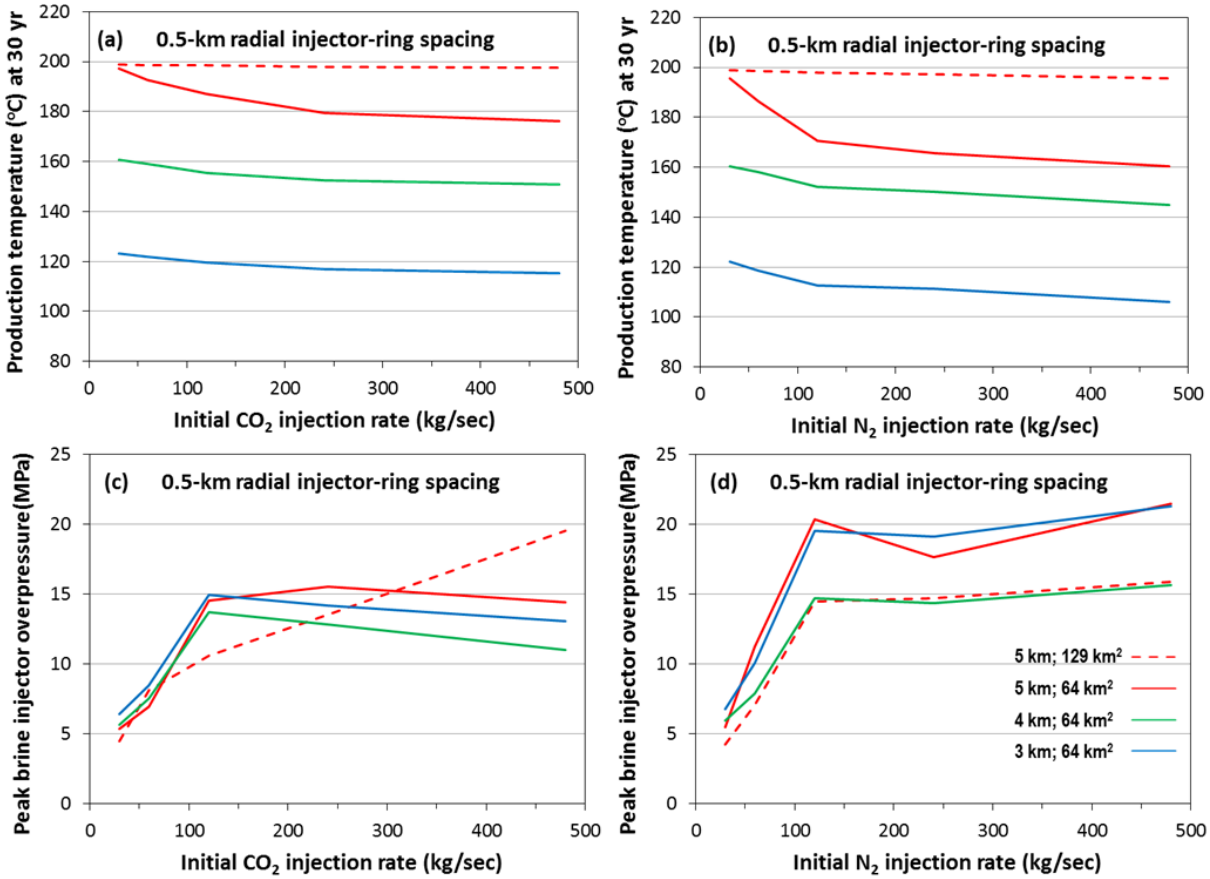

Figure 6: Production temperature at 30 yr of the outer well ring and peak brine injector overpressure for CO_2 injection (a,c) and N_2 injection (b,d) for cases with 0.5-km radial injector ring spacing. Cases are included for reservoir bottom depths of 3, 4, and 5 km and well-field footprint areas of 64 and 129 km^2.

5. FUTURE WORK

Based on the previous discussion, the use of CO_2 and N_2 injection each have their respective advantages; thus, staged supplemental-fluid (using both CO_2 and N_2) injection would be a useful strategy. Future work should investigate first-stage N_2 injection, followed by continuous CO_2 injection, together with cyclic N_2 injection for the purpose of bulk energy storage. An important goal would be for the inner ring of producers to first produce N_2 prior to the arrival of CO_2, which would help assure that CO_2 could be produced without flashing in the wellbore.

Future work should also consider intermittent fluid production for the purpose of dispatching power when it is demanded by the grid. Another objective would be to adjust the relative rates of supplemental-fluid and brine production to balance and improve heat sweep between (and within) the inner and outer swept zones. It will also be important to address the economics of power generation and bulk energy storage, with the cost of importing captured CO_2 versus the cost of separating N_2 from air being a key factor. Finally, future reservoir analyses should be conducted for realistic heterogeneous geologic settings.

6. CONCLUSIONS

We investigated the use of supplemental fluids (CO_2 and N_2) as pressure support and working fluids for geothermal energy production from stratigraphic reservoirs, using a unique subsurface design composed of four concentric rings of wells. These rings allow us to strategically create a hydraulic divide that constrains the migration of injected fluids and stores energy. The inner swept area is an important parameter because it is where the supplemental fluid (CO_2 or N_2) recirculates and where fluid displacement generates excess brine to be reinjected in the third well ring. The outer swept area is also an important parameter, because it is where brine is recirculated. Net power output can be improved if the ratio of the outer to inner swept areas is chosen to yield similar rates of thermal decline in the respective swept zones.

We investigated power generation and energy storage using N_2, power generation with CO_2, and the dependence of power generation and parasitic load on reservoir depth and temperature. In part because it can be an effective cushion gas, N_2 can be strategically injected to store and produce energy. On short energy-storage cycles (e.g., 20-days), gross power, parasitic load, and net power rates are virtually the same as in the constant-injection, no-storage case. On long energy-storage cycles (e.g., 1-year), net power rate fluctuates on the order of plus or minus 10 % if artesian flow rates are not throttled; however, total net power delivery is undiminished over the 30-yr production period. Moreover, if fluid production rates are throttled, net power fluctuations could be minimized. For the cases considered in this study, we found that time-shifting the parasitic load of N_2 separation and pumping can result in energy storage rates ranging from 72 to 376 MWe and energy stored per cycle ranging from 18 to 334 GWe-hr, which is large compared to current bulk energy storage technology.

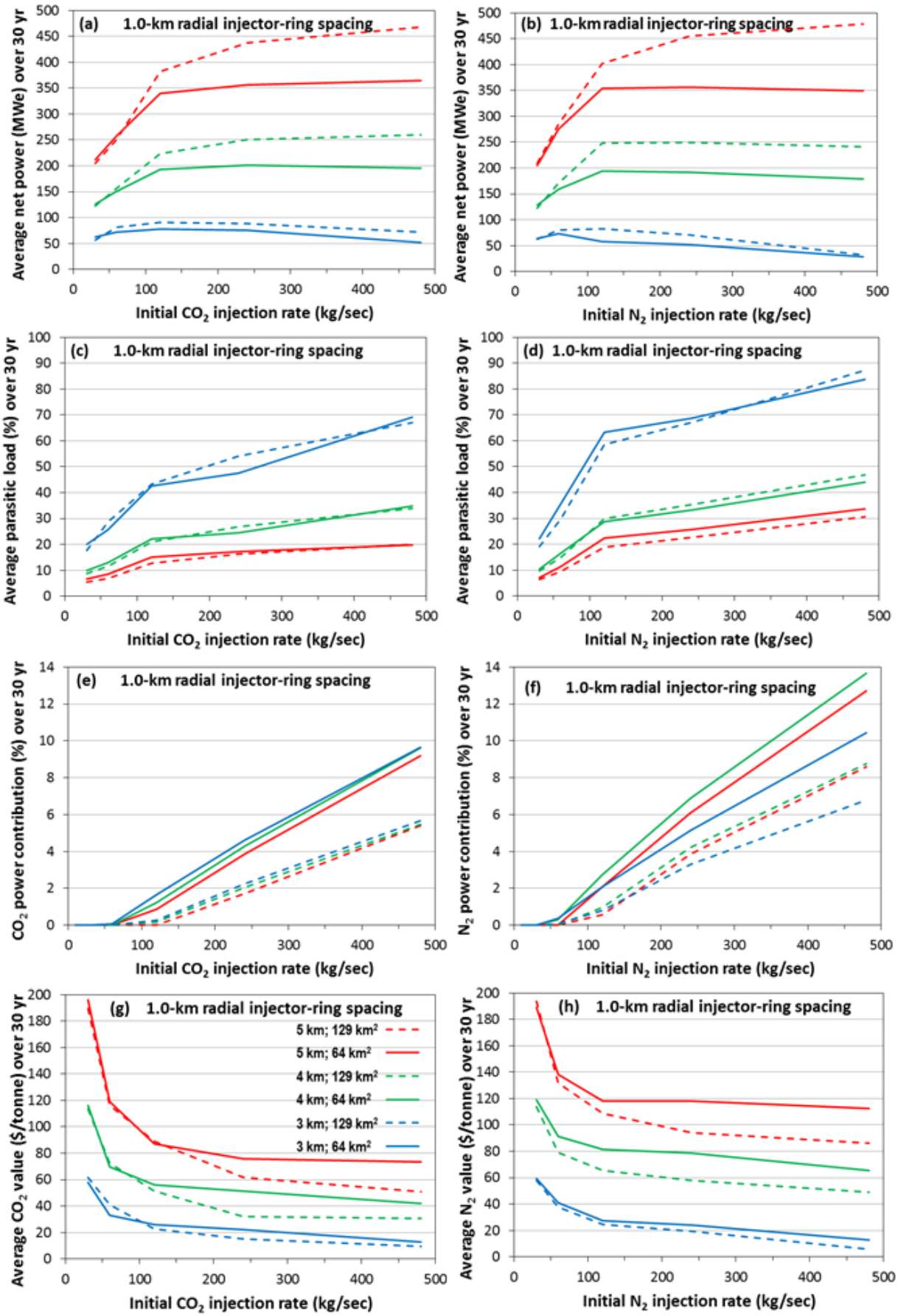

Figure 7: Power summary for CO_2 injection (a,c,e,g) and N_2 injection (b,d,f,h) for cases with 1.0-km radial injector ring spacing. Cases are included for reservoir bottom depths of 3, 4, and 5 km, and well-field footprint areas of 64 and 129 km^2. The power summary is plotted for initial CO_2 and N_2 injection rates ranging from 30 to 480 kg/sec. The average unit CO_2 and N_2 values are based on total power sales at $0.10/KWe-hr over a period of 30 yr.

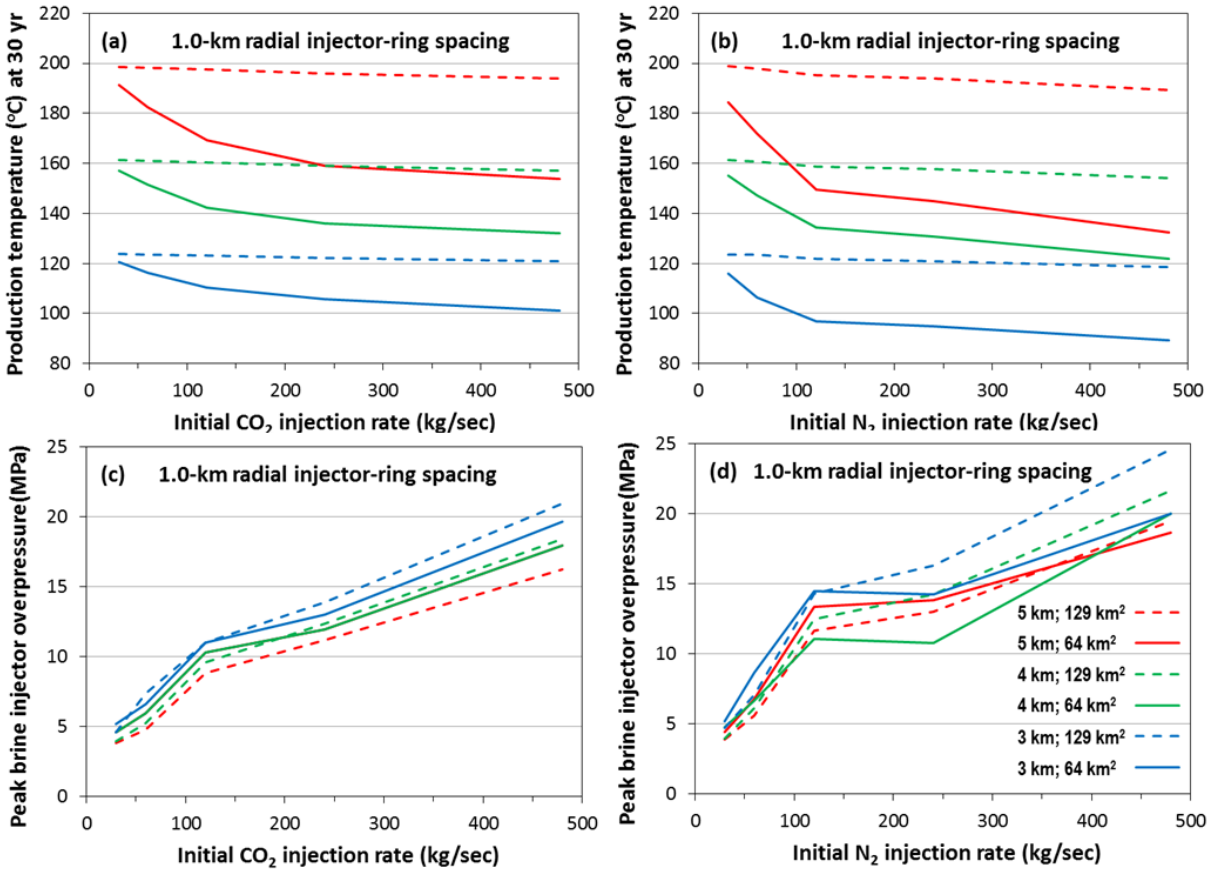

Figure 8: Production temperature at 30 yr of the outer well ring and peak brine injector overpressure for CO_2 injection (a,c) and N_2 injection (b,d) for cases with 1.0-km radial injector ring spacing. Cases are included for reservoir bottom depths of 3, 4, and 5 km and well-field footprint areas of 64 and 129 km^2.

For power generation, using CO_2 as a working fluid has a lower parasitic load and compensates for lower gross power output, resulting in nearly the same net power output as when using N_2. While N_2 is a moderately useful working fluid at high reservoir temperatures, it is counterproductive to use N_2 as a working fluid at lower temperatures, such as those associated with reservoir depths of 3 and 4 km in this study. For lower temperatures, if injected alone, N_2 should only be used for pressure augmentation of brine production.

An important finding of this study is that it requires much less supplemental fluid (CO_2 or N_2) to generate substantial net power output than previously reported. We find that a relatively small quantity of CO_2 or N_2 can create a "topographic high" in pressure, which allows overpressured brine to be injected "uphill" from the outer brine producers. This process is the subsurface equivalent of pumped-storage hydroelectricity. Subsurface "pumped storage" will drive brine production and generate highly dispatchable power, without requiring submersible pumps to lift brine. Subsurface pumped storage will also enable heat recovery to occur in hydrostatic reservoirs that are too hot (> 200°C) for submersible pumps to survive. Consequently, the unit value of CO_2 and N_2, which is quantified by total 30-yr power sales at \$0.10/KWe-hr divided by the 30-yr net storage of either CO_2 or N_2, strongly increases with decreasing supplemental-fluid rate for rates less than 120 kg/sec. For a CO_2 injection rate of 30 kg/sec, CO_2 unit value was found to be 54 to 196 \$/tonne, over the reservoir temperature range of 127.0 to 202.0°C. Such a range of unit CO_2 value could justify the cost of CO_2 capture, provided geothermal operations could be scaled to correspond to the magnitude of CO_2 capture rates associated with typical fossil-energy power plants (~120 kg/sec).

Stratigraphic reservoirs make attractive targets for geothermal development, provided the key challenges of maximizing power generation on a per well basis and minimizing the parasitic costs of fluid recirculation are met. We find that the use of CO_2 and/or N_2 as working and pressure-augmentation fluids, together with our concentric well-ring design, offers the potential to meet these challenges.

ACKNOWLEDGEMENT

This work was sponsored by the USDOE Geothermal Technologies and by the National Science Foundation. Dr. Jimmy Randolph is employed by, and has a significant financial interest in, Heat Mining Company LLC, a company that may commercially benefit from the results of this research. The University of Minnesota has the right to receive royalty income under the terms of an agreement with Heat Mining Company LLC. These relationships have been reviewed and managed by the University of Minnesota in accordance with its conflict of interest policies. This work was performed under the auspices of the USDOE by LLNL under contract DE-AC52-07NA27344.

REFERENCES

Adams, B., T.H. Kuehn, J.M. Bielicki, J.B. Randolph, and M.O. Saar, 2014. The importance of the thermosiphon effect in CO_2-Plume Geothermal (CPG) systems, *Applied Energy Journal*, in preparation.

ASME, 2006. ASME Steam Tables Compact Edition, ASME, Three Park Avenue, New York, NY, USA.

Brown, D.W., 2000. A hot dry rock geothermal energy concept using supercritical CO_2 instead of water. *Proceedings of the 25th Workshop on Geothermal Reservoir Engineering*, Stanford University, 233-238.

Buscheck, T.A., Sun, Y., Chen, M., Hao, Y., Wolery, T.J., Bourcier, W.L., Court, B., Celia, M.A., Friedmann, S.J., and Aines, R.D., 2012a. Active CO_2 reservoir management for carbon storage: Analysis of operational strategies to relive pressure buildup and improve injectivity, *Internationl Journal of Greenhouse Gas Control*, **6**, 230–245, doi:10.1.1016/j.ijggc.2011.11.007.

Buscheck, T.A., Elliot, T.R., Celia, M.A., Chen, M., Sun, Y., Hao, Y., Lu, C., Wolery, T.J., and Aines, R.D., 2012b. Integrated geothermal-CO_2 reservoir systems: Reducing carbon intensity through sustainable energy production and secure CO_2 storage*, Proceedings of the International Conference on Greenhouse Gas Technologies (GHGT-11)*, Kyoto, Japan, 18–22 Nov, 2012.

Buscheck, T.A., Chen, M., Hao, Y., Bielicki, J.M., Randolph, J.B., Sun, Y., and Choi, H., 2013b. Multi-fluid geothermal energy production and storage in stratigraphic reservoirs, *Proceedings for the Geothermal Resources Council 37th Annual Meeting*, 29 Sept–3 Oct, 2013, Las Vegas, NV, USA.

Buscheck, T.A., M. Chen, C. Lu, Y. Sun, Y. Hao, M.A. Celia, T.R. Elliot, H. Choi, and J.M. Bielicki, 2013a. Analysis of operational strategies for utilizing CO_2 for geothermal energy production, *Proceedings of the 38th Workshop on Geothermal Reservoir Engineering*, Stanford University, Palo Alto, CA, USA, 11–13 February, 2013.

Buscheck, T.A., 2014. Systems and methods for multi-fluid geothermal energy systems. US Patent Application filed.

Carr, T.R., Rich, P.M., and Bartley, J.D., 2007. The NATCARB geoportal: linking distributed data from the Carbon Sequestration Regional Partnerships. *Journal of Map and Geography Libraries: Special Issue on Department of Energy (DOE) Geospatial Science Innovations*, **4**, 131–147.

DOE, 2012. GETEM–Geothermal electricity technology evaluation model, August 2012 Beta, USDOE Geothermal Technologies Program.

Elliot, T.R., Buscheck, T.A., and Celia, M.A., 2013. Active CO_2 reservoir management for sustainable geothermal energy extraction and reduced leakage, *Greenhouse Gases: Science and Technology*, **1**, 1–16; DOI: 1002/ghg.

Fenghour, A., Wakeham, W.A., and Vesovic, V., 1998. The viscosity of carbon dioxide. *J. Phys. Chem. Ref. Data*, **27** (1), 31–44.

Hao, Y., Sun, Y., and Nitao, J.J., 2012. Overview of NUFT: A versatile numerical model for simulating flow and reactive transport in porous media, Chapter 9 in *Groundwater Reactive Transport Models*, pp. 213–240.

Lemmon, E.W. and R.T. Jacobsen, 2004. Viscosity and thermal conductivity equations for nitrogren, oxygen, argon, and air, *International Journal of Geophysics*, **25** (1), 21–69.

Nitao, J.J., 1998. "Reference manual for the NUFT flow and transport code, version 3.0," Lawrence Livermore National Laboratory, UCRL-MA-130651-REV-1, Livermore, CA, USA.

Pruess, K., 2006. Enhanced geothermal systems (EGS) using CO_2 as working fluid–a novel approach for generating renewable energy with simultaneous sequestration of carbon, *Geothermics*, **35**, 351–367.

Randolph, J.B. and Saar, M.O., 2011a. Coupling carbon dioxide sequestration with geothermal energy capture in naturally permeable, porous geologic formations: Implications for CO_2 sequestration. *Energy Procedia*, **4**, 2206–2213.

Randolph, J.B. and Saar, M.O., 2011b. Impact of reservoir permeability on the choice of subsurface geothermal heat exchange fluid: CO_2 versus water and native brine. *Proceedings for the Geothermal Resources Council 35th Annual Meeting*: 23–26 Oct, 2011, San Diego, CA, USA.

Randolph, J.B., and Saar, M.O., 2011c. Combining geothermal energy capture with geologic carbon dioxide sequestration, *Geophysical Research Letters*, **38**, L10401, doi: 10.1029/2011GL047265.

Saar, M.O., Randolph, J.B., and Kuehn, T.H., 2010. Carbon Dioxide-based geothermal energy generation systems and methods related thereto. US Patent Application 20120001429.

Span, R. and Wagner, W., 1996. A new equation of state for carbon dioxide covering the fluid region from the triple-point temperature to 1100K at pressures up to 800 MPa. *Journal of Physical and Chemical Reference Data*, **25**, 1509–1596.

Span, R., E.W. Lemmon, R.T. Jacobsen, W. Wagner, and A. Yokozeki, 2000. A reference equation of state for the thermodynamic properties of nitrogen for temperatures from 63.151 to 1000 K and pressures to 2200 MPa, *Journal of Physical and Chemical Reference Data*, **29** (6), 136–1433.

van Genuchten, M.T., 1980. A closed form equation for predicting the hydraulic conductivity of unsaturated soils. *Soil Science Society of America Journal*, **44**, 892–898.

Zhou, Q., Birkholzer, J.T., Tsang C-F., and Rutqvist, J. A., 2008.A method for quick assessment of CO_2 storage capacity in closed and semi-closed saline formations. *International Journal of Greenhouse Gas Control*, **2**, 626–639.